Modular Contact-Free Conveyors for Handling Planar Fragile Objects

Valérian Guelpa, Guillaume J. Laurent, Bassem Dahroug, and Nadine Le Fort-Piat

***Abstract*—Recent studies show that the handling of thin wafers in the photovoltaic industry can lead to unacceptable yields due to cell scratching and breaking. This paper presents the concept and design of a novel modular conveyor that is intended for handling planar fragile objects at a high speed without contact. Each element of the conveyor is a square block that is able to generate tilted air jets that lift and push the object in a single direction. Various handling functions can thus be achieved by the assembly of several blocks. To manage the complexity of assembling systems composed of hundreds of blocks, an automatized design methodology is proposed. This process gives the best topology of the conveyor that meets expected specifications such as trajectory, speed, and travel time. The optimization relies on the physical model of the modular system describing the motion of the object pushed by directed air jets. Experimental comparisons show that the simulation predicts accurately the motion of a glass wafer according to the arrangement of the blocks and the volume of air flow. A maximal speed of 0.3 m/s was experimentally observed and, on larger simulated conveyors, the speed of the wafer could theoretically reach 2.9 m/s.**

***Index Terms*—Air film manipulation, contactless handling, distributed manipulation, modular design, wafer handling.**

I. Introduction

TODAY, the vast majority of photovoltaic (PV) solar cells are still based on crystalline silicon wafers. This technology is expected to remain dominant for at least ten years [1]. As raw silicon is expensive and in short supply, the main challenges for the PV industry are to improve the efficiency and effectiveness of resource consumption through raw materials reduction, improved cell concepts, and automation of manufacturing [2]. This has led the PV industry to follow the semiconductor industry in finding ways to make thinner substrates [3].

But recent industrial studies have shown that the use of thin wafers can lead to unacceptable yields arising from wafer and cell breakage due to handling during production [4]. Indeed, as wafer thickness decreases, wafers are less stable and more vulnerable to stresses, and dies can be prone to breaking and scratching especially during handling between machines [5].

Conventional wafer-transfer systems use comb pairs to lift wafers out of carriers and comb assemblies to retain the wafers. The low thickness of the wafers and their sharp edges make it difficult to consistently position the combs, which ultimately can cause wafer breakage [3]. Bernoulli grippers are also widely used as noncontact end effectors for "gentle handling." But Bernoulli grippers still need some means of holding the wafer so it does not drift around as the gripper moves it. Moreover, when handling thin wafers, the low pressure tends to deform the wafer and can lead to cracks and wafer breakage [4].

Low-cost thin wafer handling has been identified as one of the difficult challenges in the 2013 International Technology Roadmap For Semiconductors Roadmap [6]. To address these challenges, new wafer handling technologies have to be developed.

An alternative solution is to levitate the substrate. For instance, air bearings are widely used to transport large, thin, and heavy products like glass and LCD panels [7], [8]. Instead of pressurized air fed through orifices or porous media, ultrasound bearings can also be used to lift a substrate over a vibrating plate [9]–[12]. But air bearing and vibrating tables realize only the levitation of product; the lateral motion is still realized by another principle (gravity, wheels, belt conveyors).

To move wafers, a set of inclined holes can create an air flow in addition to the air cushion under the object. Combination of several nozzles with different orientations can produce different functions such as transfer track, position control track, orientation control track, etc.

This paper presents a novel concept of a contact-free conveyor for transporting planar fragile objects like silicon wafers, solar cells, glass and LCD panels, paper sheets, etc. This conveyor is intended to fulfill various functions such as moving, capturing, guiding, centering, rotating, etc. As opposed to very complex devices dedicated to one task and motion, we propose a modular approach based on simple unidirectional blocks that can be assembled together to perform the desired function. This concept, covering all the handling functions in a single design, allows cost reduction and the making of various and large conveyors.

To manage the complexity of assembling such modular systems, we also propose a general and automatized methodology that gives the topology of the conveyor according to given industrial specifications. To this end, we express the block arrangement problem into an optimization problem. This planning phase is carried offline during the design of the production line and before its implementation. This optimal design methodology relies on an accurate physical model of tilted air jet levitation and propulsion.

The main contributions of this paper are as follows

1) the concept and design of a contact-free modular conveyor;

Manuscript received June 21, 2016; revised August 30, 2016; accepted September 4, 2016. This paper was recommended for publication by Associate Editor M. Yim and Editor I. M. Chen upon evaluation of the reviewers' comments. This work was supported in part by the Smart Blocks Project under Grant ANR-251-2011-BS03-005, in part by the Labex ACTION Project under Grant ANR-11-LABX-01-01, and in part by the Franche-Comté Region.

The authors are with the FEMTO-ST Institute, Université de Bourgogne Franche-Comté, UFC/ENSMM/CNRS, Besançon 25000, France (e-mail: valerian.guelpa@femto-st.fr; Guillaume.Laurent@ens2m.fr; bdahroug@gmail.com; npiat@ens2m.fr).

Color versions of one or more of the figures in this paper are available online at http://ieeexplore.ieee.org.

Digital Object Identifier 10.1109/TRO.2016.2623340

2) a complete physical model of the dynamics of the object propelled by air jets, the proposed model being carefully validated with experiments;
3) an automatic design methodology able to find the best topology addressing a given set of specifications.

This paper is organized as follows. The modular concept is presented in Section II. Section III presents the physical modeling, its software implementation, and its experimental validation. In Section IV, we propose a method to automatically design conveyors based on a optimization procedure. Section V concludes the paper.

II. Modular Conveyor

This section introduces the modular concept after a short presentation of related works. An exhaustive survey on air film transportation has been published previously in [13].

A. Air Film Wafer Transportation

The first attempts to use air films to transport and position wafers were carried out at Texas Instruments Corporation by Hagler [14] and at IBM by Hassan and Paivanas [15], [16]. Toda *et al.* [17], [18] improved the concept and made a transfer system for 300 mm wafer. The wafer track consists of a perforated plate with 0.5 mm-diameter tilted holes. Transport times of less than 15 s, from wafer moving at 0.12 $m{\cdot}s^{-1}$ to wafer stopping, were achieved in the 0.8-m-long wafer transport track.

Similar systems have been investigated by Moon and Hwang [19] and by Kim and Shin [20], [21]. Kim and Shin proposed some methods to compute the precise position on the wafer with cheap photo proximity sensors but no experimental performances are reported. Arrays of tilted air jets have been used to transport various thin products. For instance, the Xerox PARK handling system [22], [23] uses 1152 directed air jets in a 12 in. $\times$ 12 in. array to levitate paper sheets. The system has demonstrated closed-loop trajectory tracking with typical velocity about 30 $mm{\cdot}s^{-1}$.

In [24] and [25], Wesselingh *et al.* introduced a new concept of wafer positioning based on an array of cells able to generate an air film for both suspension and motion. Their device is dedicated to wafer micropositioning. A servo error of 20 μm (P-P) and a positioning repeatability of 3 μm (STD) were reported with low-cost optical sensors that detect the edge of the wafer [26].

Luntz and Moon [27], [28] and Varsos *et al.* [29], [30] proposed another principle based on potential air flow to move an object on an air-hockey table. Their method allows the movement of an object to a unique final pose using airflow fields without sensors. Laurent *et al.* [31]–[33] used a similar traction principle to move a product using an array of vertical air jets to induce desired potential air flow over the surface. This device is able to move centimeter-sized objects up to 0.2 $m{\cdot}s^{-1}$ with millimeter closed-loop positioning accuracy.

The proposed solutions are often too slow to meet industrial high throughput demands. For example, recent PV processing machines can reach throughput rates of 15 000 wafers per hour, leading to velocities up to 2 $m{\cdot}s^{-1}$ in a serial flux (with two wafers by meter in the line).

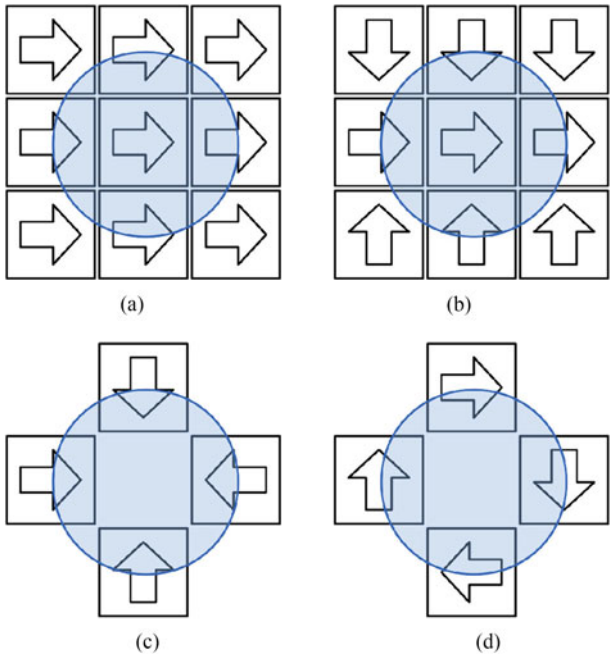

Fig. 1. Illustration of the modular concept. The assembly of unidirectional blocks can induce various motions to the object (here a circular wafer). (a) Simple motion, (b) guided motion, (c) positioning, and (d) rotation.

In addition, these devices are all designed to achieve a dedicated task whereas wafer handling requires a lot of different trajectories to sort, serialize, or parallelize the flow between batch and nonbatch processing machines [34]. This lack of functionality and versatility multiplies the different kinds of systems to be installed, thus raising problems of maintenance, complexity of the production line, etc.

Some authors have proposed a modular approach to address these issues in the case of wheeled conveyors [35]–[38]. The underlying idea is that complex conveyors can be made by the assembly of several simple modules. Particular trajectories and behaviors are then obtained by composing design patterns. A contactless conveyor made of modules, termed "blocks," will allow equally the realization of different kinds of functions with a single design. However, we will see that the design pattern approach is inadequate for contactless systems and automated synthesis methods will be needed.

B. Modular Concept

To reduce the cost of production, the blocks must also have a very simple design. Among the mentioned possibilities to move an object on an air cushion, an array of tilted air jet is the simplest solution. Accordingly, we propose the use of square blocks in which the upper surfaces contain an array of tilted holes with the same angular orientation. Indeed, a single such block can push the object in a determined direction. The assembly of unidirectional blocks can induce various motions to object, as illustrated in Fig. 1.

On the one hand, having identical and modular blocks makes them easier and cheaper to produce. On the other hand, designing too small modules could dramatically increase the complexity of the assembly and the cost of a conveyor.

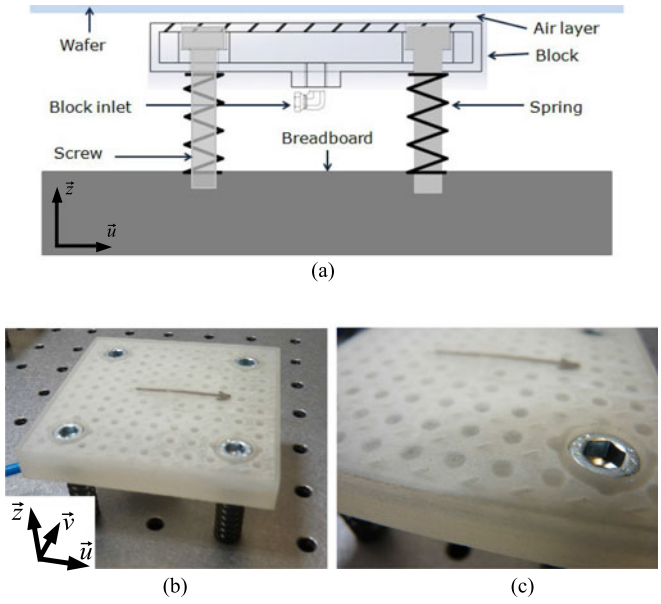

Fig. 2. Design of the blocks. The jets are oriented in the direction $\vec{u}$. (a) Cross view of a module, (b) picture of a 3-D printed module, and (c) detailed view of inclined jets.

Actually, the size of the blocks must be adapted to the shapes and dimensions of the transported objects. The goal is to design the largest modules that can together perform all the desired handling functions. If the size of a block is over the half of the object size, the object will cover less than the half of a block for some functions such as positioning and guided motion. Using smaller covered surfaces could affect the efficiency of the guidance. That's why having a block which side is equal to half of the object size is a good compromise. In other words, this size is the largest one that allows all the required functions of complex conveyors, such as moving, guiding, positioning, and rotating to be fulfilled.

C. Block Design

In this paper, we used 150 mm glass wafers to demonstrate the potentiality of the approach but others planar objects with different materials and shapes could be transported as well.

To handle 150 mm circular wafers, the blocks are preferred to have a dimension of 75 mm $\times$ 75 mm. The blocks have been fabricated by 3-D printing, as shown in Fig. 2(b). The upper surface of the blocks contains 128 holes with tilt angles of 45°. The jet diameter is preferred to be 0.5 mm because of the resolution restrictions of the 3-D printer. The blocks are attached on a breadboard using four screws and four springs in order that the block surface can be adjusted to be perfectly horizontal, as illustrated in Fig. 2(a).

III. Physical Modeling and Simulation

The realization of an optimal conveyor requires understanding the underlying physics. In this section, we present the physical modeling of the conveyor and the implementation of its simulation. Finally, we experimentally prove the relevancy of the model.

A. Physical Modeling

1) Levitation Height: A general assumption for the modeling of air-bearing tables is that the fluid is incompressible since the pressure used is only several kilopascals, near atmospheric pressure. The lifting force exerted against the object can by divided in two components. The first one, the aerodynamic lift force, is the result of the collision of the air jet with the lower face of the object. The momentum-flux conservation for one jet P along the direction z gives

$$\vec{F}_{L_1}(P) = \rho q_e U_e \cos(\theta)\vec{z} = \rho \frac{q_e^2}{a}\cos(\theta)\vec{z} \tag{1}$$

where ρ is the fluid density, $q_e = U_e a$ the supplied gas flow rate, U_e the exit speed of gas in nozzle, θ the inclination angle of the hole from the vertical, and a the section area of a hole.

In air-bearing tables, the aerodynamic force is usually negligible with respect to the aerostatic component. The aerostatic force is due to the distribution $p(x, y)$ of pressure beneath the substrate. The pressure distribution is very complex in general, especially since the air jets from the table impinge on the underside of the object at various points nonsymmetrically. Even for simple case such as a disk centered on a single hole, an exact solution of the Navier–Stokes equation appears to be difficult.

In [39], McDonald proposed a solution for a disk centered on a single hole assuming that the velocity is purely radial and in which the nonlinear term of the Navier–Stokes is ignored. McDonald's original equations depend on pressure differences between the center and the edge of the disk. For practical reasons, we rewrote it in terms of volumetric inflow as

$$p(r) = \frac{6\mu q_e}{\pi h^3}\ln\frac{r_d}{r} \tag{2}$$

where r_d is the radius of the disk, r the distance to the hole (with $r > r_i$, the hole radius), μ the dynamic viscosity of air, and h the levitation height. This approximate solution is valid if

$$\frac{\rho h q_e}{24\pi\mu r^2} \ll 1. \tag{3}$$

In practice, the approximation holds everywhere except in the immediate vicinity of the nozzle. Thus, by integrating the pressure over the lower surface of the disk, we get the aerostatic lift force

$$\vec{F}_{L_2} = \frac{3\mu q_e S}{\pi h^3}\vec{z} \tag{4}$$

where $S = \pi r_d^2$ is the surface of the disk.

This equation stands for a disk centered on a single vertical hole on a thin air film but experiments show that it is a reasonable approximation for a disk covering multiple tilted holes and at low flow rates. $\vec{F}_{L_2}$ is thus calculated with the sum of the flow of the air jets that impinge on the underside of the object. Finally, for an object at rest covering k tilted holes, the levitation height is the solution of

$$mg\vec{z} + \vec{F}_{L_2} + \sum_{i=1}^{k}\vec{F}_{L_1}(P_i) = 0 \tag{5}$$

with m the object mass and g the standard gravity.

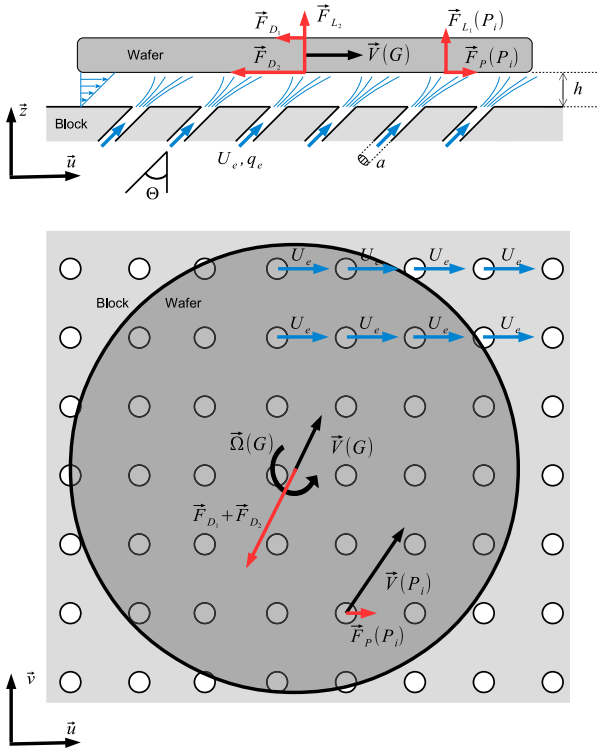

Fig. 3. Principle and modeling of tilted air jet handling (not to scale).

2) Propulsion Force: The object is propelled by the action of tilted air jets (cf., Fig. 3). A synthetic model of air jets has been proposed by Toda *et al.* [17]. The tangential force F_P exerted by a sole covered jet onto the object can be calculated according to

$$\vec{F}_P(P) = \frac{1}{2}\rho C_p a \sin(\theta) \left\| U_e - \vec{V}(P)\cdot\vec{u} \right\|^2 \vec{u} \tag{6}$$

where C_p is a dimensionless coefficient, $\vec{V}(P) = \vec{V}(G) + \overrightarrow{PG} \wedge \vec{\Omega}$ is the velocity of the object over the position P of the jet and $\vec{u}$ is the direction of the jet in the $O\vec{x}\vec{y}$ plane. The torque applied to the object by a jet can also be calculated as

$$\vec{\tau}_P(P) = \overrightarrow{GP} \wedge \vec{F}_P(P) \tag{7}$$

with G the center of mass of the object.

3) Drag Forces: When moving on the air-bearing object, it is slowed down by the air resistance. The resistance force is the sum of the frictional resistance acting on the upper surface, the drag force acting on the edge, and the frictional resistance acting on the underside (cf., Fig. 3).

In the case of handling thin object like wafers, the drag force acting on its edge can be neglected since its thickness is very low. The frictional resistance acting on the upper surface is also weak and can be approximated by

$$\vec{F}_{D_1} = -C_f S \vec{V}(G) \tag{8}$$

with $\vec{V}(G)$ being the velocity of the center of mass of the object and C_f being a dimensionless coefficient.

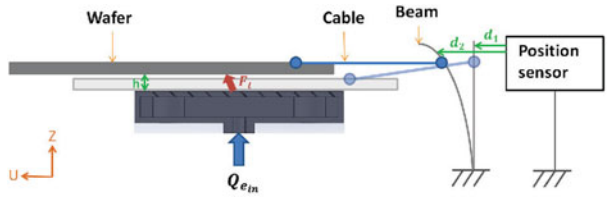

Fig. 4. Diagram of the setup used to determinate the coefficient C_p.

The main frictional resistance is located on the underside and can be described as Couette's flow and calculated by

$$\vec{F}_{D_2} = -\frac{\mu S}{h}\vec{V}(G). \tag{9}$$

The drag torque is obtained by

$$\vec{\tau}_D = -\vec{\Omega}(C_f + \frac{\mu}{h})I_z \tag{10}$$

with $\vec{\Omega}$ the angular velocity and I_z the area moment of inertia of the object ($I_z = \frac{\pi}{2}r_d^4$ for a disk).

4) Equation of Motion: Finally, the equations of the motion of the object on k tilted air jets are

$$m\vec{A} = \vec{F}_{D_1} + \vec{F}_{D_2} + \sum_{i=1}^{k} \vec{F}_P(P_i) \tag{11}$$

and

$$I\vec{\alpha} = \vec{\tau}_D + \sum_{i=1}^{k} \vec{\tau}_P(P_i) \tag{12}$$

where $\vec{A}$ is the object acceleration, $\vec{\alpha}$ is its angular acceleration, and I is its moment of inertia ($I = mr_d^2$ for a disk).

B. Coefficient Identification

In order to measure the propulsion coefficient C_p we realized a specific setup to measure the force applied to a glass wafer by four blocks. To identify the resulting force as a function of the air flow rate, a thin metallic beam is fixed alongside a contactless displacement sensor (see Fig. 4). This sensor measures the displacement δ of the beam when it is bent by an applied force. The wafer and the beam are connected with a cable to allow vertical motion of wafer. Finally, the wafer is placed over four blocks to begin the experiment.

Since the horizontal motion of the wafer is constrained by the beam, the summation of horizontal forces is equal to zero when the wafer velocity is null along the u axis. As a result, the force applied by k air jets to the wafer can be determined, knowing the stiffness coefficient K_b of the beam, by

$$k \cdot \vec{F}_P = K_b \delta \vec{u}. \tag{13}$$

Thus, the propulsion coefficient can be calculated using (6)

$$C_p = \frac{2K_b\delta}{\rho k a U_e^2 \sin\theta} = \frac{2aK_b\delta}{\rho k q_e^2 \sin\theta}. \tag{14}$$

Several tests were done, each one with a different wafer mass in order to observe the influence of levitation height on results (see Fig. 5). This stiffness K_b, here equal to 348.8 N$\cdot$ m^{-1}, has

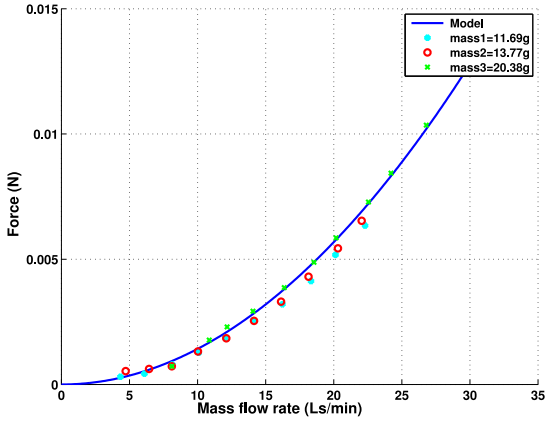

Fig. 5. Force applied on the beam in function of the total inflow rate. The first test series "." was done with a wafer of mass 11.69 g, the second test series "o" with a mass of 13.77 g, and the last "*" with a mass of 20.38 g. The continuous line represents the modeled propulsion force.

been measured beforehand using calibrated weights. The mean value of C_p that fits the data (in a least-squares sense) is $C_p = 12.1$. Moreover the good accordance of the curves confirms the relevancy of the model and that the propulsion coefficient is independent of the levitation height.

C. Experimental Validation

To validate the model, we realized some comparisons between experimental trials and predicted results. The prediction is performed by observing the state of the real experiment at the step time k, then by simulating the time $k+1$ (one step ahead prediction). In the experiments, the sampling time between these two states is 1/15 s (corresponding to the frame rate of the camera used to measure the wafer position).

The first validation setup is a configuration of 21 blocks generating a linear trajectory of the wafer with an acceleration and a deceleration phase [see Fig. 6(a) and 6(b)]. The air flow in each block is set to 5 L$\cdot$ min^{-1}.

The displacement of the wafer from one side to the other side of the setup is observed. If the predictions at $k+1$ are compared with the experimental results, Fig. 6(c) is obtained.

Table I gives the standard deviations of prediction errors. As the errors depend on the time step, we computed the relative prediction errors defined by the ratio between the norm of the prediction error and the norm of the effective displacement between two time steps. The mean relative prediction error of the simulation is around 3.5% of the displacement. This value qualifies the good agreement between the simulation and the experiment.

The second setup used is a configuration of 12 blocks, generating a circular trajectory when the wafer is released from an unstable position [see Fig. 7(a)]. The air flow in each block is still set to 5 L$\cdot$ min^{-1}.

Fig. 7(b) shows the predictions and the experimental results according to time. For this experiment, the relative prediction error is 5.7%.

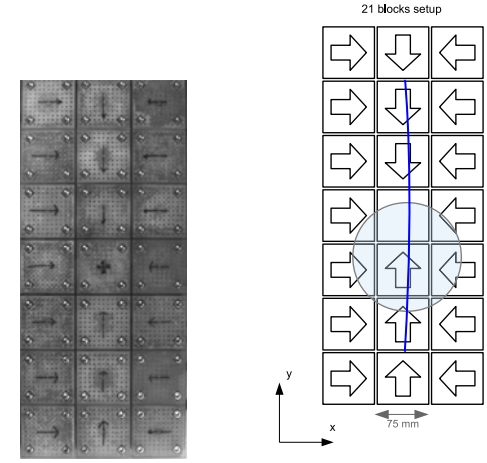

(a) (b)

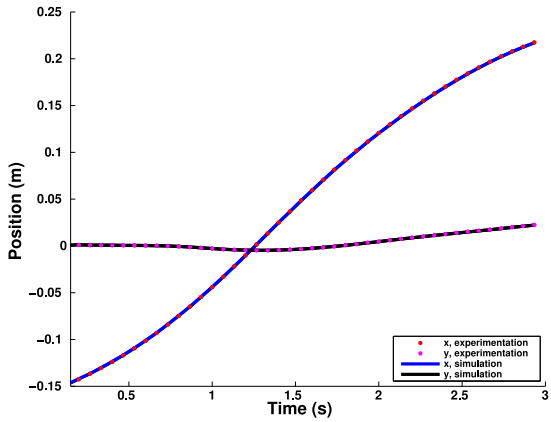

(c)

Fig. 6. Comparison between simulation and experimentation on the 21-block setup. (a) Picture of the 21-block setup and (b) Configuration of the blocks. The blue curve presents the experimental trajectory.

TABLE I
STANDARD DEVIATION AND RELATIVE VALUES OF THE PREDICTION ERROR PRESENTED IN FIG. 6 AND FIG. 7

Linear experiment		Circular experiment	
Absolute error	Std (m)	Absolute error	Std (m)
x axis	$9.3119 \cdot 10^{-5}$	x axis	$3.3388 \cdot 10^{-5}$
y axis	$2.3083 \cdot 10^{-4}$	y axis	$2.4850 \cdot 10^{-5}$
Relative error		Relative error	
Simulation	3.5%	Simulation	5.7%
Free motion	10.4%	Free motion	29.6%

These results have been also compared with a simple predictor used as benchmark. This predictor gives the position and speed of the wafer at time $k+1$ as the natural evolution of the state k without external forces or dissipation (free motion). Fig. 7(c) shows the error between both predictions and the experimental results. The relative error of the free-motion predictor reaches

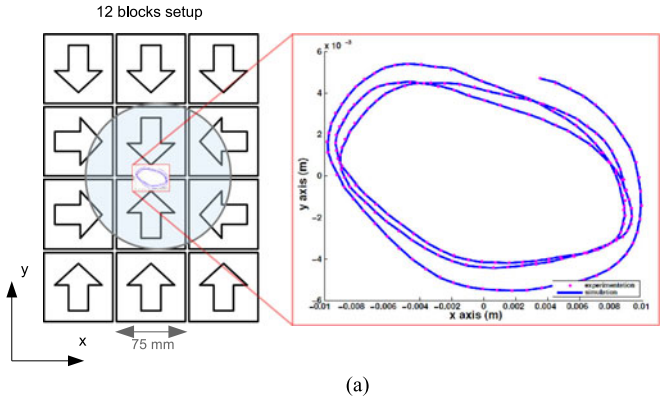

(a)

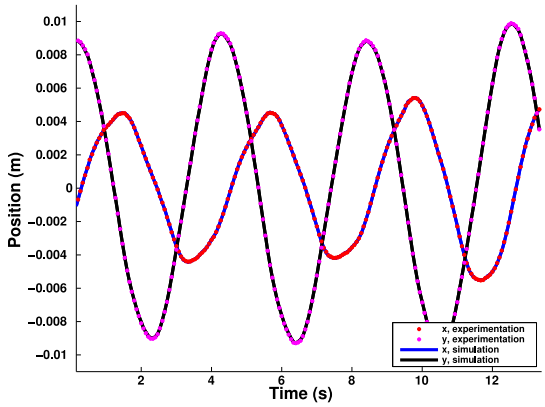

(b)

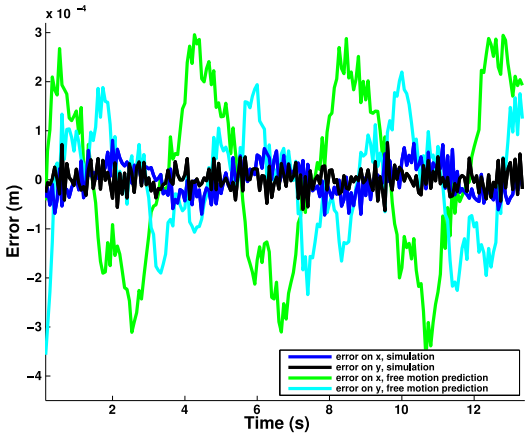

(c)

Fig. 7. Comparison between simulation and experimentation on the 12-block setup. (a) Real and predicted trajectories on the 12-block setup, (b) predictions and measurements versus time, and (c) errors between the prediction and the experimental measurements.

29.6%. This last comparison demonstrates that the model predicts accurately the object dynamics. Table I sums up the relative prediction errors for both experiments and both predictors.

IV. Optimal Design

The implementation of a large modular conveyor that meets specifications in terms of trajectory and throughput is a complex

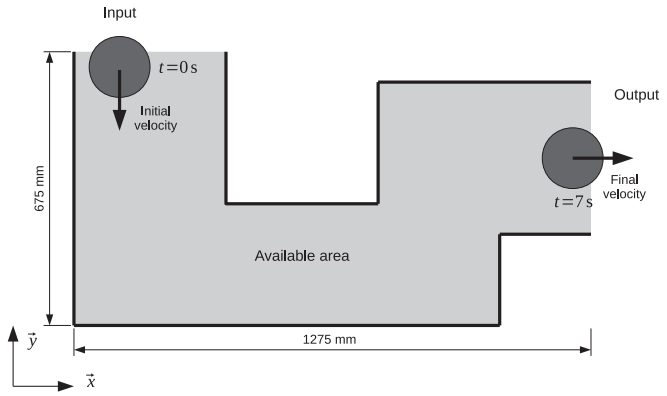

Fig. 8. Illustration of the case study. Blocks are placed around the obstacles (in gray) and randomly initialized. The aim is to go from the beginning position to the ending position, with a specific final velocity, and in 7 s (the specifications are $x^*(0) = 0$ m, $y^*(0) = -0.15$ m, $\dot{x}^*(0) = 0$ m$\cdot$ s^{-1}, $\dot{y}^*(0) = -0.3$ m$\cdot$ s^{-1}, $x^*(7) = 1.125$ m, $y^*(7) = -0.375$ m, $\dot{x}^*(7) = 0.3$ m$\cdot$ s^{-1}, $\dot{y}^*(7) = 0$ m$\cdot$ s^{-1}).

problem. The aim is to find the orientation and inflow value of each block that produces the closest experimental trajectory to the desired one. In this section, we first try to find a spatial configuration by composing simple design patterns. This brings to the conclusion that the search of a setup corresponding to accurate specifications is not feasible by hand. Thus, we propose a general and automatized methodology that gives the topology of the conveyor according to given specifications.

A. Patterning

We propose a case study based on a typical conveying task that can occur between two nonbatch processing machines in the PV industry. An illustration of this case study is presented in Fig. 8.

The wafer is brought on the roller belt of a first processing machine to a starting point with an initial velocity of 0.3 m$\cdot$ s^{-1}. The objective is to feed a second machine at an given point and with the same velocity. To make the problem more complex, the wafer has to avoid some obstacles and has to finish the displacement at a specific time (7 s).

As a first approach, we try to comply with these specifications by combining simple design patterns (like those illustrated in Fig. 1). The airflow rates are manually set, that requires a hundred of tries before to obtain a satisfying solution. Fig. 9 shows the best solution obtained by this way. In addition to being burdensome, the time criterion is not reached: the displacement takes more than 15 s. The final position is acceptable but the speed along x-axis is only 0.2 m$\cdot$ s^{-1} and the speed along the y-axis is not null. To conclude, the patterning approach can be used only to design simple trajectories such as straight lines but is not suitable to large and complex conveyors. In the following, we propose a computational methodology based on the optimization of the conveyor topology.

B. Decision Domain

We consider that the setup is initially composed of regularly placed blocks, covering the whole available area.

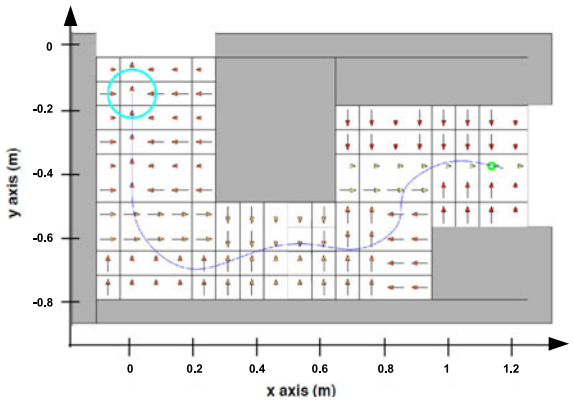

Fig. 9. Trajectory of the wafer (center position) for the patterning solution generated by disposing blocks patterns. The darker the color of the arrows, the stronger the air flow of the block.

Then, the angular position and the air flow of each block required to meet the specifications must be determined. After the optimization, when the optimal path would be found, the useless blocks that are not on the trajectory can be removed.

The orientation (yaw angle α_i) of each block i can take four discrete values, $\alpha_i \in \{0; \pi/2; \pi; 3\pi/2\}$. The air flow $q_{e,i}$ of each block i is a continuous variable and could be taken between a minimal value allowing the levitation and a maximal value depending on the block limitations, $q_{e,i} \in [q_{e,\min}; q_{e,\max}]$. So, for a setup with N blocks, there are $2N$ decision variables mixing discrete and continuous values

$$D = [\alpha_1, \alpha_2, \ldots, \alpha_N, q_{e,1}, q_{e,2}, \ldots, q_{e,N}]. \tag{15}$$

C. Objective Function

To define the objective function, we first consider that the production context imposes some goals: the object must be moved along a trajectory defined by different points (start, end, etc.), the object must have a defined velocity at certain locations (for example at the ending point), the object must avoid obstacles and other objects, if any are in the path, and finally, the system must meet some global criteria such as air consumption.

Some constraints, such as not hitting something, do not have any tolerance. The other objectives, such as the ending position and velocity, may be more or less close to the defined value, depending on the production needs.

To balance these different goals, the objective function is composed of the sum of squared errors of criteria

$$J(D) = \sum_i w_i * c_i^2 \tag{16}$$

where c_i is a criterion and w_i is a weighting coefficient.

A small set of criteria is sufficient to address most of the applications. First, criteria can be defined on the position of the object at a given time. For instance, if the specifications require that the object reaches the abscissa $x^*(t)$ at time t, the associated criterion can be defined by

$$c_i = x(t) - x^*(t). \tag{17}$$

Similar criteria can be written to specify the ordinate, the angular position, and also the velocity at a given time such as

$$c_i = \dot{x}(t) - \dot{x}^*(t). \tag{18}$$

Acceleration requirements can be equally addressed with this kind of criterion.

Some global criteria can also be defined such as global air consumption, the total travel time, the number of useful blocks, etc. For instance, the total air consumption is given by

$$c_i = \sum_j^N q_{e,j}. \tag{19}$$

It is noteworthy that for a given set of criteria, the weights can be modified according to the need, selecting the desired solution on the Pareto frontier.

D. Optimal Design

One of the challenges raised by this optimization problem is that its high-dimension decision space, which embeds a lot of local optima, has to be explored. For these reasons, we used the genetic algorithm from MATLAB's Global Optimization Toolbox with built in crossover and mutation operators. The fitness and the genotype are respectively defined by (16) and (15). As the tiling of the useful area consists of 122 blocks, the genotype D has 244 decision variables in this case of study.

For this task, two initial criteria require that the position $(x(7), y(7))$ of the wafer's center at time $t = 7$ s has to be the nearest to point $(x^*(7), y^*(7))$. The two last criteria state that the speed $(\dot{x}(7), \dot{y}(7))$ of the wafer's center at same time has to be the closest to the speed $(\dot{x^*}(7), \dot{y^*}(7))$. The objective function is then

$$\begin{aligned} J(D) = \; & w_1 * (x(7) - x^*(7))^2 + w_2 * (y(7) - y^*(7))^2 \\ & + w_3 * (\dot{x}(7) - \dot{x^*}(7))^2 + w_4 * (\dot{y}(7) - \dot{y^*}(7))^2. \end{aligned} \tag{20}$$

We choose to give more importance to the respect of specified position and speed along the *y*-axis than along the *x*-axis through the choice of the weighting coefficients: $w_1 = 2, w_2 = 4, w_3 = 0.1$, and $w_4 = 0.8$.

Fig. 10(a) presents the trajectories of the center of the wafer for initial population of the optimization process, composed of 200 random configurations. Fig. 10(b) illustrates the progression of the algorithm after 100 generations. The best solution found allows the desired conveying function to be generated by removing unused blocks [see Fig. 10(c)].

In our case, the errors between obtained values and expected values are: $x(7) - x^*(7) = -5.15 \cdot 10^{-5}$ m, $y(7) - x^*(7) = 1.96 \cdot 10^{-5}$ m, $\dot{x}(7) - \dot{x}^*(7) = 1.70 \cdot 10^{-3}$ m$\cdot$ s^{-1}, and $\dot{y}(7) - \dot{y}^*(7) = -7.05 \cdot 10^{-5}$ m$\cdot$ s^{-1}. These precisions are far better than the industrial needs. Furthermore, the discrepancies between the errors illustrates the importance of the weighting coefficients.

Of course, a different choice of weights could induce a different Pareto-efficient solution. For example, by giving more

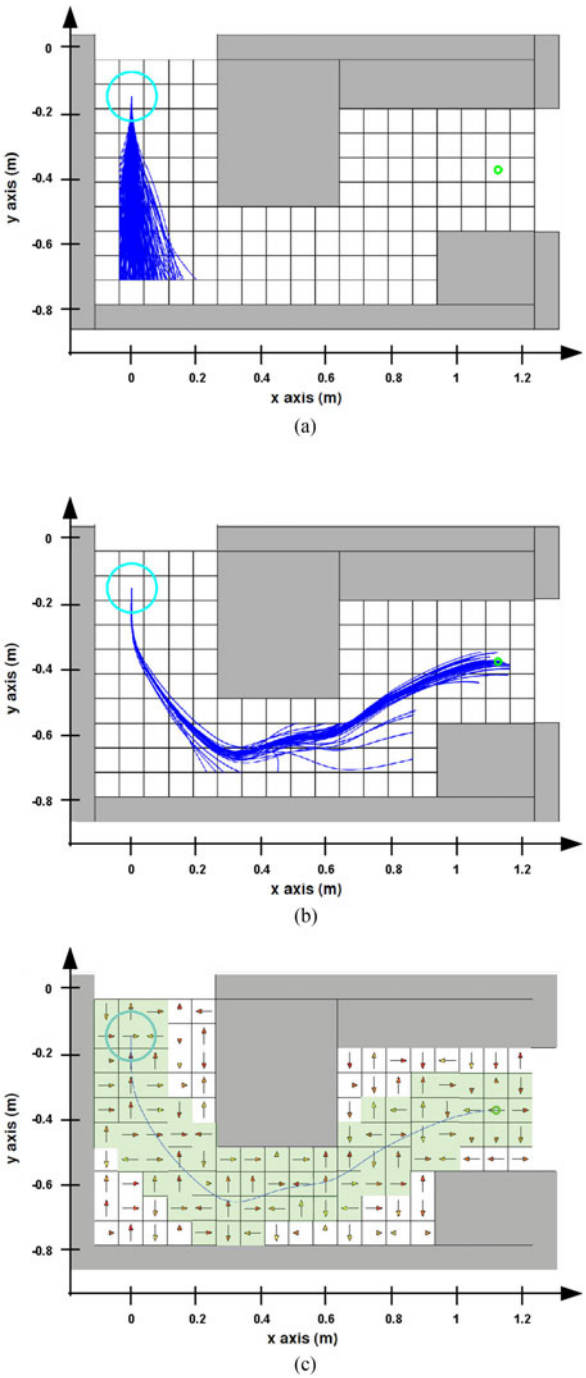

Fig. 10. Trajectories of the wafer (center position) for the different solutions generated by the genetic algorithm. Each generation includes 200 individual solutions. (a) Trajectories of the wafer for the initial population of the genetic algorithm. This population is randomly generated. (b) Progress of the genetic algorithm after 100 generations and (c) final solution of the genetic algorithm (i.e., the best solution at generation 100). The darker the color of the arrows, the stronger the air flow of the final solution. The green blocks are those useful to implement the conveyor.

weight to the position, we can obtain a better final positioning precision at the expense of velocity objectives. The choice of a solution on the Pareto frontier would have to be made by the production engineer.

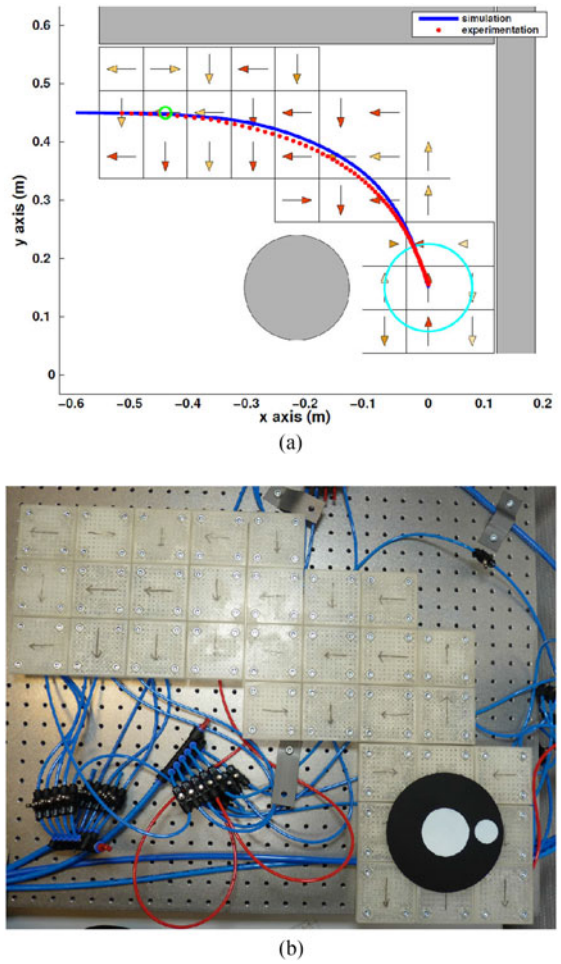

Fig. 11. Experimental validation of the methodology. (a) Trajectory of the wafer on the conveyor obtained with the genetic algorithm. The graphs represent the simulated result and the experimental result with the same setup. The darker the color of the arrows, the stronger the air flow. (b) Picture of the real setup used for the validation.

E. Experimental Validation

In order to validate the proposed optimization methodology, we carried out an L-shaped setup with 33 physical blocks. This setup is smaller than that one presented previously in case study because of the number of available blocks.

The goal is to reach a final position from an initial position without initial speed and avoiding obstacles. The wafer must reach the ending position as quickly as possible and with a zero speed along the y-axis. In this way, the objective function is defined by

$$J(D) = 1 * (x(t) - x^*(t))^2 + 1 * (y(t) - y^*(t))^2 + 0.1 * (\dot{y}(t) - \dot{y^*}(t))^2 + 0.0001 * t^2 \quad (21)$$

with t the travel time before collision or before reaching the abscissa of the target.

Fig. 11(a) presents the trajectory of the best result obtained by simulation (in blue). Then, we test this solution on the setup by using a flow meter to adjust the air flow of the blocks as recommended by the genetic algorithm. The red curve of Fig. 11(a)

TABLE II
RESULTS OF SIMULATION AND EXPERIMENTATION ON THE L-SHAPED SETUP

For $t = 3.8$ s	Simulation	Experimentation
$x(t)$ (m)	-0.4449	-0.4400
$y(t)$ (m)	0.4456	0.4468
$\dot{x}(t)$ (m·s^{-1})	-0.3064	-0.3050
$\dot{y}(t)$ (m·s^{-1})	0.0223	0.0158

corresponds to the experimental trajectory on the real conveyor [see Fig. 11(b)].

Simulated and experimental results are well correlated: the curves are close together and the final speed of the wafer along the x-axis is near -0.3 m·s^{-1} in both cases (see Table II). Nevertheless, there is a slight difference between the simulated and experimental paths. Indeed, as the system is not in closed loop, the external perturbations (which are not predictable) can cause a divergence between the simulated and experimental trajectories. External perturbations are mainly due to ambient air streams. Also, the hand setting of each block (inclination and air flow rate) is not perfect and can induce some discrepancies between the model and the reality.

V. CONCLUSION

In this paper, a new concept of a modular conveyor using air bearing has been presented. The air-bearing principle allows the handling of planar fragile objects like silicon wafers on complex trajectories at a high speed without damage. In addition, the modular nature of the conveyor produces benefits in the ease of realization of each block and the simplification of maintenance. However, the large number of elements in each conveyor requires automatized research of the best configuration to address given specifications.

To overcome this complexity, a systematic method based on an optimization procedure has been proposed. A small set of criteria allows the task to be defined with high flexibility: users can change the objectives and the weights according to the needs (e.g., to improve speed, positioning accuracy, or to reduce air consumption). Experiments have also demonstrated that the generated solutions are feasible and reliable.

A maximal speed of 0.3 m·s^{-1} was experimentally observed. Moreover, thanks to the simulation, we can estimate the speed for larger conveyors. For instance, the speed of a circular wafer could theoretically reach 2.9 m·s^{-1} with a maximal acceleration of 0.48 m·s^{-2} (at the start) on a 1-m-long track made of 15 $\times$ 3 blocks (without initial velocity). These values overcome the requirements in terms of throughput for the considered industrial applications.

REFERENCES

[1] I. E. Agency, Ed., *Solar Photovoltaic Energy Technology Roadmap*, 2010. [Online]. Available: https://www.iea.org/publications/freepublications/publication/pv_roadmap.pdf

[2] R. Leachman, S. Ding, and C.-F. Chien, "Economic efficiency analysis of wafer fabrication," *IEEE Trans. Autom. Sci. Eng.*, vol. 4, no. 4, pp. 501–512, Oct. 2007.

[3] L. Teschler, "Next big challenge for PV makers: Wafer handling," *Machine Design*, vol. 80, no. 13, 2008. [Online]. Available: http://machinedesign.com/archive/next-big-challenge-pv-makers-wafer-handling

[4] X. F. Brun and S. N. Melkote, "Analysis of stresses and breakage of crystalline silicon wafers during handling and transport," *Sol. Energy Mater. Sol. Cells*, vol. 93, pp. 1238–1247, 2009.

[5] J. N. Burghartz, Ed., *Ultra-Thin Chip Technology and Applications*. New York, NY, USA: Springer, 2011.

[6] *Assembly and Packaging Difficult Challenges*. International Technology Roadmap For Semiconductors, 2013.

[7] M. Hoetzle, T. Dunifon, and L. Rozevink, "Glass transportation system," U.S. Patent 6 505 483, 2003.

[8] H. G. Lee and D. G. Lee, "Design of a large {LCD} panel handling air conveyor with minimum air consumption," *Mechanism Mach. Theory*, vol. 41, no. 7, pp. 790–806, 2006. [Online]. Available: http://www.sciencedirect.com/science/article/pii/S0094114X05001710

[9] G. Reinhart *et al.*, "Non-contact handling and transportation for substrates and microassembly using ultrasound-air-film-technology," in *Proc. IEEE/SEMI Adv. Semiconductor Manufacturing Conf.*, 2011, pp. 1–6.

[10] J. Höppner and J. Zimmermann, "Device for contactlessly gripping and positioning components," US Patent 6647791, Nov. 2003. [Online]. Available: http://www.freepatentsonline.com/6647791.html

[11] M. Schilp, J. Zimmermann, and A. Zitzmann, "Device for non-contact transporting and holding of objects or material," US Patent 2011/0311320, Dec. 2011. [Online]. Available: http://www.freepatentsonline.com/y2011/0311320.html

[12] J. Zimmermann, D. Jacob, and A. Zitzmann, "Device for conveying and positioning of structural elements in non-contact way," US Patent 7260449, Aug. 2007. [Online]. Available: http://www.freepatentsonline.com/7260449.html

[13] G. J. Laurent and H. Moon, "A survey of non-prehensile pneumatic manipulation surfaces: principles, models and control," *Intell. Service Robot.*, vol. 8, no. 3, pp. 151–163, 2015. [Online]. Available: http://dx.doi.org/10.1007/s11370-015-0175-0

[14] R. G. Hagler, "Transporting and positioning system," US Patent 3717381, 1973.

[15] J. K. Hassan and J. A. Paivanas, "Pneumatic control of the motion of objects suspended on an air film," US Patent 4165132, 1979.

[16] J. A. Paivanas and J. K. Hassan, "Air film system for handling semiconductor wafers," *IBM J. Res. Develop.*, vol. 23, no. 4, pp. 361–375, 1979.

[17] M. Toda *et al.*, "N_2 tunnel wafer transport system," *J. Inst. Environ. Sci.*, vol. 40, no. 1, pp. 23–28, 1997. [Online]. Available: http://iest.metapress.com/content/35810332n0552006/?referencesMode=Show

[18] M. Toda, M. Umeda, Y. Kanno, and T. Ohmi, "Floating apparatus of substrate," eP Patent 1005076, May 2000. [Online]. Available: http://www.freepatentsonline.com/EP1005076A1.html

[19] I.-H. Moon and Y.-K. Hwang, "Evaluation of a wafer transportation speed for propulsion nozzle array on air levitation system," *J. Mech. Sci. Technol.*, vol. 20, no. 9, pp. 1492–1501, 2006.

[20] Y.-J. Kim and D. H. Shin, "Wafer position sensing and motion control in the clean tube system," in *Proc. IEEE Int. Conf. Ind. Technol.*, 2006, pp. 1315–1319.

[21] D. H. Shin, H. G. Lee, and H. S. Kim, "Wafer positioning control of clean tube system," in *Proc. ACSE Conf.*, Dec. 2005, pp. 203–207.

[22] A. A. Berlin *et al.*, "Motion control of macro-scale objects using large-area arrays of MEMS-like distributed manipulators," presented at 7th Mechatronics Forum Int. Conf., Atlanta, GA, Sep. 6–8, 2000.

[23] D. K. Biegelsen *et al.*, "Air-jet paper mover: An example of meso-scale MEMS," *Proc. SPIE*, vol. 4176, pp. 122–129, 2000.

[24] J. Wesselingh, R. van Ostayen, J. Spronck, R. Schmidt, and J. van Eijk, "Actuator for contactless transport and positioning of large flat substrates," in *Proc. Eur. Soc. Precision Eng. Nanotechnol. Int. Conf.*, 2008, pp. 145–149.

[25] J. van Rij, J. Wesselingh, R. A. J. van Ostayen, J. Spronck, R. M. Schmidt, and J. van Eijk, "Planar wafer transport and positioning on an air film using a viscous traction principle," *Tribology Int.*, vol. 42, pp. 1542–1549, 2009.

[26] J. Wesselingh, J. Spronck, R. van Ostayen, and J. van Eijk, "Contactless 6 dof planar positioning system utilizing an active air film," in *Proc. Eur. Soc. Precision Eng. Nanotechnol. Int. Conf.*, 2010.

[27] J. Luntz and H. Moon, "Distributed manipulation with passive air flow," in *Proc. IEEE/RSJ Int. Conf. Intell. Robot. Syst.*, 2001, pp. 195–201.

[28] H. Moon and J. Luntz, "Distributed manipulation of flat objects with two airflow sinks," *IEEE Trans. Robot.*, vol. 22, no. 6, pp. 1189–1201, Dec. 2006.

[29] K. Varsos and J. Luntz, "Superposition methods for distributed manipulation using quadratic potential force fields," *IEEE Trans. Robot.*, vol. 22, no. 6, pp. 1202–1215, Dec. 2006.
[30] K. Varsos, H. Moon, and J. Luntz, "Generation of quadratic potential force fields from flow fields for distributed manipulation," *IEEE Trans. Robot.*, vol. 22, no. 1, pp. 108–118, Feb. 2006.
[31] G. J. Laurent, A. Delettre, and N. L. Fort-Piat, "A new aerodynamic traction principe for handling products on an air cushion," *IEEE Trans. Robot.*, vol. 27, no. 2, pp. 379–384, Apr. 2011.
[32] A. Delettre, G. J. Laurent, Y. Haddab, and N. L. Fort-Piat, "Robust control of a planar manipulator for flexible and contactless handling," *Mechatronics*, vol. 22, no. 6, pp. 852–861, 2012.
[33] A. Delettre, G. J. Laurent, N. L. Fort-Piat, and C. Varnier, "3-DOF potential air flow manipulation by inverse modeling control," in *Proc. IEEE Int. Conf. Autom. Sci. Eng.*, 2012, pp. 926–931.
[34] L. Li, Z. Sun, M. Zhou, and F. Qiao, "Adaptive dispatching rule for semiconductor wafer fabrication facility," *IEEE Trans. Autom. Sci. Eng.*, vol. 10, no. 2, pp. 354–364, Apr. 2013.
[35] J. E. Luntz, W. Messner, and H. Choset, "Distributed manipulation using discrete actuator arrays," *Int. J. Robot. Res.*, vol. 20, no. 7, pp. 553–583, 2001.
[36] M. Bedillion and W. Messner, "Control for actuator arrays," *Int. J. Robot. Res.*, vol. 28, no. 7, pp. 868–882, 2009.
[37] K. Furmans, C. Nobbe, and M. Schwab, "Future of material handling—Modular, flexible and efficient," in *Proc. IEEE/RSJ Int. Conf. Intell. Robot. Syst.*, 2011.
[38] T. Kruhn, M. Radosavac, N. Shchekutin, and L. Overmeyer, "Decentralized and dynamic routing for a cognitive conveyor," in *Proc. 2013 IEEE/ASME Int. Conf., Adv. Intell. Mechatron.*, 2013, pp. 436–441.
[39] K. T. McDonald, "Radial viscous flow between two parallel annular plates," 2000. [Online]. Available: https://arxiv.org/abs/physics/0006067

Valérian Guelpa received the Graduate degree in mechanics and microtechnologies from National School of Mechanics and Microtechnologies, Besançon, France, and the Master's degree in mechatronics, microsystems, and embedded electronics from University of Franche-Comté, Besançon, France, in 2013. He is currently working toward the Ph.D. degree in the Department of Automatic Control and Micromechatronic Systems, FEMTO-ST Institute, Besançon, France, where his research involves microrobotics and visual measurements.

Guillaume J. Laurent received the Engineer's degree in mechanics in 1999 and the Ph.D. degree in control systems and computer sciences in 2002, both from University of Franche-Comté, Besançon, France.

He is an Associate Professor with National School of Mechanics and Microtechnology, Besançon, France.

He is a member of the Department of Automatic Control and Micromechatronic Systems, FEMTO-ST Institute, Besançon, France. His research interests are in microrobotics, micromanipulation, distributed manipulation, and vision for microrobotics.

Bassem Dahroug received the B.Sc. degree in mechanical engineering from Arab Academy for Science, Technology & Maritime Transport, Alexandria, Egypt, in 2011 and the M.Sc. degree in mechatronics and micromechatronics system from National School of Mechanics and Microtechnology, Besançon, France, and EPI, Gíjon, Spain, in 2014. He is currently working toward the Ph.D. degree in the AS2M Department, FEMTO-ST Institute, where his research is focused on design and control of microrobot for middle ear surgery.

Nadine Le Fort-Piat received the Ph.D. degree in control systems and signal processing from University of Technology of Compiégne (UTC), Compiégne, France, in 1984.

She became an Associate Professor with UTC in 1984 and a Professor with National Engineering School of Mechanics and Microtechnologies, Besançon, France, in 1998. She is a member of the Department of Automatic Control and Micromechatronic Systems, FEMTO-ST Institute, Besançon, France. Her research is in the perception and advanced control strategies based on visual servoing for micro and nanomanipulation.